


Review

Material Reuse in Laser Powder Bed Fusion: Side Effects of the Laser—Metal Powder Interaction

Eleonora Santecchia *, Stefano Spigarelli and Marcello Cabibbo

Dipartimento di Ingegneria Industriale e Scienze Matematiche (DIISM), Università Politecnica delle Marche, Via Brecce Bianche 12, 60131 Ancona, Italy; s.spigarelli@univpm.it (S.S.); m.cabibbo@univpm.it (M.C.)

* Correspondence: e.santecchia@univpm.it; Tel.: +39-0712204731

Received: 1 February 2020; Accepted: 1 March 2020; Published: 4 March 2020



Abstract: Metal additive manufacturing is changing the way in which engineers and designers model the production of three-dimensional (3D) objects, with rapid growth seen in recent years. Laser powder bed fusion (LPBF) is the most used metal additive manufacturing technique, and it is based on the efficient interaction between a high-energy laser and a metal powder feedstock. To make LPBF more cost-efficient and environmentally friendly, it is of paramount importance to recycle (reuse) the unfused powder from a build job. However, since the laser–powder interaction involves complex physics phenomena and generates by-products which might affect the integrity of the feedstock and the final build part, a better understanding of the overall process should be attained. The present review paper is focused on the clarification of the interaction between laser and metal powder, with a strong focus on its side effects.

Keywords: LPBF; laser radiation; metal powder; spatter; condensate

1. Introduction

Metal additive manufacturing (AM) is a cluster of technological processes which allow building tridimensional objects by adding material, instead of subtracting it, as happens during traditional manufacturing [1,2]. A direct consequence of this new construction paradigm is a radical change of mentality in terms of component design, since it allows realizing geometrical shapes which could be totally new and also inspired by nature (bioinspired, biomimetic, organic design [3]). This freedom of design not only allows optimizing the geometries and reducing the weight of the final parts, but also has a big impact on the final cost of the single part, which is mainly determined by the amount of material used to build the component. Moreover, since complexity comes without additional costs, the production of lattice structures [4–6] is advisable and opens the door to shape optimization, oriented to foster multi-functionality by combining, for example, protective and thermal properties (i.e., heat exchangers) [7].

The most common metal additive manufacturing processes use pure or pre-alloyed metal powders with micrometric dimensions, which can vary according to the process and the high-intensity beam used to melt the powder (i.e., laser or electron beam).

Laser powder bed fusion (LPBF) is the most used metal AM technology worldwide. Equipment based on this technology includes a powder delivery system, where the metal powder feedstock is loaded, and the build chamber, where the final part is built in a layer-upon-layer fashion, using a high-energy laser (typically a single-mode continuous-wave solid-state fiber laser operating at a wavelength of 1075 nm) which selectively fuses the powder according to a given computer-aided design (CAD) model. During the process (Figure 1), the metal powder is spread from the delivery system by a recoater blade, while the build platform, mounted on a piston, is lowered to a height having the same value as the thickness of the slice to be melted. The process is repeated layer after

layer until the final part is obtained. It is worth noting that the LPBF process is typically performed under inert gas (argon or nitrogen) atmosphere, with a continuous gas flow [8].

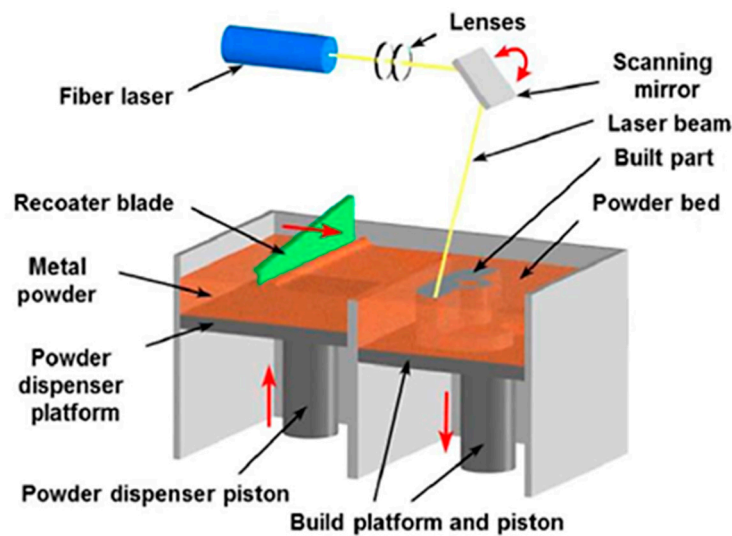


Figure 1. Schematics of the laser powder bed fusion (LPBF) equipment. Adapted from Reference [9] with permission from Elsevier.

While the market and the applications of laser powder bed fusion continuously and impressively grew in recent years, there is a common view across users and researchers concerning the repeatability of the process in terms of chemical composition and mechanical properties of the final parts, which are of paramount importance when challenging environmental or testing conditions are considered [10–16].

The most typical approach to study the microstructural and mechanical properties of parts built by LPBF is to compare them with castings of the same alloy or, rather, the corresponding alloy since the starting material is metal powder rather than a fuse. However, in some existing alloys designed for cast and wrought parts, laser additive manufacturing processing results in cracking or other microstructure deficiencies [11,12,16,17]. It is worth noting that LPBF has more similarities with laser welding rather than casting, since the two laser-based techniques have some common features (i.e., melt-pool formation, moving heat source) [18]. However, process parameters are, in general, quite different in terms of laser power and scan speed, and the laser–matter interaction is much more complicated in LPBF processes, since the powder feedstock is inherently unstable and the solidified material undergoes multiple thermal cycles corresponding to the fusion of subsequent layers during the additive process [19–22]. Furthermore, owing to the similarities with welding and to the complicated interaction between laser and metal particles, when comparing laser powder bed fusion with other metal forming processes, it is evident that the range of processable alloys is very limited and the number of high-productivity commercially available alloys is even smaller [23]. One of the reasons behind this is that the level of metal powder sensitivity to the laser action during LPBF is not yet fully understood, despite the efforts of the scientific community to uncover it [24–27], and the same applies to the final mechanical properties of the built parts. A direct consequence is that reused and sieved powder is sometimes seen as a risk affecting the repeatability of the mechanical properties, producing expensive waste.

The price of the metal powder feedstock is indeed quite high, such as up to several hundreds of United States dollars (USD) per kilogram (i.e., ~\$400 USD/kg for Ti-6Al-4V) and, since typically only a small percentage of the total powder contained in the machine dispenser is actually used to build the part (only 10–50% of the build volume), without a proper recycling strategy, the cost of the powder in the finished part could be doubled [28–31].

The interaction between the high-energy laser typical of LPBF equipment and the metal powder bed can result in powder contamination through different phenomena including agglomeration, partial fusing, partial/full oxidation, metal vapor condensate, and generation of spatter [32–40]. These phenomena can alter not only the properties of the reused powder (i.e., flowability, chemical composition, tap density, particle size), but also the surface (i.e., roughness), microstructural (i.e., local variation of chemical composition, pore formation), and mechanical properties of the final part.

For these reasons, the present review paper aims to shed light on the interaction between laser and metal powder, with a strong focus on its side effects, which could affect the chance to recycle the powder feedstock and the following reliability of LPBF-built parts.

2. The LPBF Process

The powder bed is a layer of powder characterized by a packing density (which depends on the arrangement of the particles and the unfilled areas between them), which is then subjected to the action of the laser, which melts the requested areas of the bed. The remaining unmelted powder serves, layer-upon-layer, as additional support to the part under construction, and some areas of the bed close to the laser action can be heated several times during the overall process.

The interaction between the metal powder and the laser radiation during the process is associated with energy deposition following the powder coupling (absorption of radiation by metal particles, which appear as gray bodies due to their morphology) and bulk coupling (absorption of radiation by a metallic surface, related to the intrinsic properties of the considered metal) mechanisms [41,42]. The optical penetration is often evaluated comparing the powder bed to a bulk, but this is not completely right. The interaction with particles can, indeed, generate multiple reflections [43,44], which enhance the penetration depth of the laser. Since the action of the laser is very short in time and characterized by a very high energy (resulting cooling rates of about $\sim 10^5$ – 10^6 K/s [45]), evaporation and melting of the exposed powder particles can easily occur [46,47].

In addition to studying the full LPBF process to realize parts and samples for tensile and fatigue tests, single-track experiments are extensively used to understand the powder–laser interaction [48–51]. These experiments allow highlighting the presence of stability zones, where the track is continuous, and instability zones, whose irregularities (i.e., distortions, balling) are highly dependent on the scanning speed values, on the laser power, on the thickness of the powder layer and the substrate material on which it is spread, and on the powder particle morphology and granulometry [33,42,46,48,52–54].

2.1. Powder Feedstock Features

The quality of samples and parts built with laser powder bed fusion is strongly influenced by the properties of the metal powders particles themselves [30,55,56], as also outlined by official regulation agencies such as ASTM (ASTMF2924-14 [29]). Granulometry, flowability, particle size, density, and chemical composition are among the most crucial properties which are typically checked before processing the selected powder [47,57–61].

The quality and properties of the feedstock materials depend a lot on the manufacturing process, which, in the case of metal powders for LPBF, can be quite varied [18,62–67], ranging from rotary, water, and gas atomization [66–70] to the plasma rotating electrode process (PREP) [71,72]. Furthermore, in order to make the additive manufacturing process more cost-efficient and to reduce the price of the feedstock, the reuse of scraps and chips produced by traditional manufacturing of expensive metals and alloys (i.e., Ti-6Al-4V, aluminum) was proposed via spheroidization [73,74] and milling [75,76].

The literature shows that powder recycling, when referring to the LPBF process, can be done in a variety of ways [23,77], ranging from the reintroduction of sieved powder after each build and adding the used and sieved powder together with the virgin one with or without mixing, to the mixing of used powder with powder of the same age after each cycle (defined as the number of jobs after which the amount of feedstock is not enough to perform further jobs). According to literature, the first two procedures seem to be the most used [19,78–81]. Denti et al. [30] recently suggested a parameter called

“average usage time” (AUT) to account for the real duration of laser–powder interaction, instead of the number of jobs performed, which could be widely adopted as a reliable method to evaluate the level of interaction. Modifications of powder properties with reuse in LPBF are highly influenced by the starting material, the process parameters, and the environment inside the build chamber. In the case of highly reactive powders (i.e., Al- and Ti-based powders), even the storage and handling conditions might affect the quality of the powder [82].

What is most striking from the results performed on many different alloys (stainless steels, Ti-6Al-4V, AlSi10Mg, IN718 and IN625, Co–Cr, Scalmalloy) [19,30,37,58,82–88], in terms of reused powder characterization and, most importantly, of the microstructural and mechanical properties of the final parts, is that, while the former are quite similar for the same alloy, the latter are characterized by very scattered results [23]. Mechanical properties could be improved, decreased, or unaffected by the reuse of feedstock material, as shown by the results reported in Table 1. This result suggests that more attention should be paid to what really happens inside the chamber during the laser–powder interaction and not only to the metal powder quality itself.

Table 1. Summary of studies on powder recycling (IED—input energy density, UTS—ultimate tensile strength, ND—not determined).

Material	Reuse Times (Max)	Reuse Strategy	IED (Linear) (P/v) (J/m)	Tensile Properties (UTS)	Charpy	Fatigue Life	Reference
Ti-6Al-4V	12	Sieving	ND	Virgin: 1030 MPa Reused: up to 1101 MPa but plateau at 1072 from 6 to 12 reuses	ND	ND	[79]
Ti-6Al-4V	31	Powder sampled from trap capsules (double cone shape); sieving	ND	Virgin: 984.3 ± 0.6 Reused: 1002.7 ± 1.2 (all samples subjected to hot isostatic pressing)	ND	ND	[85]
Ti-6Al-4V	15	Sieving	233.3	Comparable	ND	No differences in as-built condition Longer life with the reused powder at a strain of 0.004 mm/mm with machined surface condition	[87]
Ti-6Al-4V	ND	Sieving	ND	Comparable	Decrease with reuse	ND	[78]
Ti-6Al-4V	100	Addition of virgin powder when needed	233.3	Scattered results but no decrease (stress relieved samples)	ND	ND	[30]
IN718	14	Sieving and drying	ND	ND	Variations with the number of reuses but no clear trend	ND	[19]
IN718	10	Sieving	ND	Consistent from build to build (samples were stress-relieved, hot isostatically pressed, solution-treated, and aged)	ND	Comparable low cycle fatigue	[8]
AlSi10Mg	1	Sieving	284.6	Comparable	ND	ND	[83]
AlSi10Mg	1	Sieving	284.6	Comparable	ND	ND	[88]
AlSi10Mg	8	Sieving	ND	Decrease with reuse	ND	High cycle fatigue decreases with reuse	[81]

Table 1. Cont.

Material	Reuse Times (Max)	Reuse Strategy	IED (Linear) (P/v) (J/m)	Tensile Properties (UTS)	Charpy	Fatigue Life	Reference
AlSi10Mg	18	Sieving	284.6	No effects	ND	ND	[80]
17-4 PH	1	Sieving	237.5	Similar trend for spatter-rich and non-spatter-rich samples. Abrupt failure for spatter-rich samples and 5% lower ductility	ND	ND	[89]
17-4 PH	10	Sieving	243.7	Similar UTS but failure strain of print 10 parts decreased by ~7%.	ND	ND	[40]

2.2. Heat Source

The interaction between metal powder particles and laser radiation during LPBF is quite complex and includes a number of physical phenomena, such as chemical reactions and phase transformation, heat transfer, and a complex fluid flow within the melt pool due to the surface-tension gradient, as well as absorption and scattering of the laser radiation [18]. The high-energy solid-state lasers typically employed in LPBF have an axisymmetric Gaussian profile of the power density distribution, with beam diameters between 50 and 100 μm for fine resolution, and an intensity which decreases upon penetration through the powder layers deposited on top of each other [41,48,90], since the radiation also penetrates through the pores between the particles in the bed.

The connection between the shape of the laser beam profile and the melt pool was extensively studied in the literature [51,91,92]. Furthermore, the top-hat shape employed in laser welding [93] was shown to produce keyholes having a shorter depth and, for this reason, Tenbrock et al. [94] recently applied this profile in laser powder bed fusion of 316 L stainless steel, showing that an efficient LPBF processes can also be realized by applying diode lasers as long as a proper defined intensity threshold is exceeded ($I \approx 8\text{--}10 \times 10^5 \text{ W/cm}^2$ [94]).

The use of ultrafast lasers (i.e., femtosecond lasers) is also under study since they could allow processing metal and alloys with high melting temperatures and thermal conductivity (i.e., rhenium) and ceramics [95,96].

2.3. Shielding Gas Flow

The laser powder bed fusion process is always performed under inert atmosphere, in order to avoid any possible interaction between the metal particles (very reactive with a high specific surface area) and impurities such as humidity and light elements (i.e., oxygen, carbon oxides), which might affect the local chemical composition and the resulting mechanical properties of the manufactured parts [18,23,58]. Furthermore, a continuous flow of inert gas is essential in order to limit the redeposition on the powder bed of by-products during the process; this is crucial because should the removal of by-products by the shielding gas flow not be effective, there is a high risk of laser attenuation [97–99]. Owing to the formation of metal vapor plume during the laser–powder interaction, the incident laser energy could be absorbed partially. These effects were particularly studied by Grünberger and Domröse [100], who generated the so-called splashy process by changing the focal position of the laser and concluded that a proper gas flow rate is mandatory in order to avoid the occurrence of this phenomenon, since, in areas of the build chamber where the local gas flow velocity is slow, there is a higher beam scattering. The gas flow in the process chamber was found to be a crucial parameter to limit the presence of defects in parts obtained by laser powder bed fusion [97,101].

The most used inert gases are argon and nitrogen, although, in the case of highly reactive materials prone to nitride formation, Ar is the only available option [102]. However, Pauzon et al. [103] recently studied combinations of Ar and He to process Ti-6Al-4V, and their results showed improved cooling rates and an impressively higher build rate (up to 40%).

3. Side Effects of Laser–Metal Powder Interaction

In order to account for the process parameters having a tangible influence on the laser–powder interaction, one of the most typical ways is to use a parameter called the input energy density (IED, J/cm^2), calculated as shown in Equation (1).

$$IED = \frac{P}{(v \cdot d)}, \quad (1)$$

where P is the laser power, v is the scan speed, and d is the laser beam diameter [104,105]. Sometimes Equation (1) is slightly modified when referring to a linear specimen ($IED = P/v$) [106,107]. While similar properties are expected when IED is fixed but its variables change [9,32,108–110], Guo et al. [20]

showed that the effect of laser power and scan speed should be evaluated differently since they could lead to different laser–powder interaction results.

In order to account more for the process parameters which lead the LPBF process, energy density can be defined as volumetric and calculated as a function not only of the laser power (P) and scan speed (v), but also of the layer thickness (t) and hatch spacing (h), as outlined in Equation (2) [9,42].

$$IED = \frac{P}{v \cdot h \cdot t}. \quad (2)$$

Typically, when laser and powder particles come in contact during a laser powder bed fusion process, several phenomena can occur at the same time (Figure 2) and can be further classified as denudation and generation of the heat-affected powder (spatter and condensate).

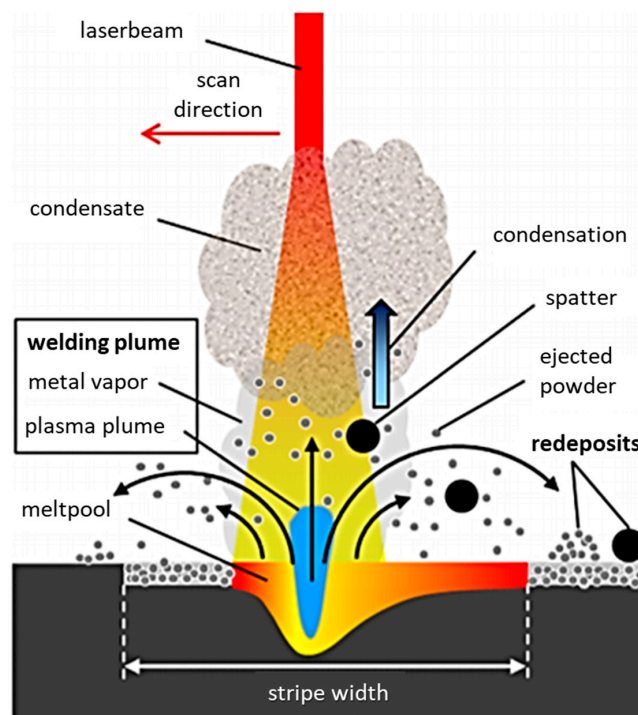


Figure 2. Schematics of LPBF process by-products formation. Adapted from Reference [97] with permission from Elsevier.

3.1. Denudation

Denudation is a term which defines the formation of apparent clearing zones around a single laser track, as shown in Figure 3.

This complex phenomenon is based on the interaction between the rapidly formed melt pool, which generates tracks with a width larger than the incident laser diameter [34], owing to the surface tension which spreads the molten metal and the surrounding particles of the powder bed. The temperature gradient between regions on the surface of the melt pool generates the undesired Marangoni flow which dominates the transition region together with the vapor recoil momentum, pulling in the melt-pool-adjacent particles, creating the denudation zone [22,33,111]. As shown in Figure 3, there is an area around the laser heat zone where the vaporization of elements indeed generates the entrainment of powder particles (Bernoulli effect).

Denudation is highly dependent on the gas flow pressure and on laser parameters (power and speed). In the former case, Matthews et al. [34] showed that the correlation with the Knudsen number (Kn , defined as the ratio of the mean free path of the gas molecules to the length scale of the considered system) outlined how the gas flow affects the size of denudation area and the height of the laser scan

track. When Kn is lower than 1, powder particles are drawn in the melt pool or ejected upward, while, for Kn values higher than 1, the vapor plume will expand, pushing the particles outward. High values of laser power and speed generate a thin melt pool which, in turn, gives rise to the humping phenomenon (periodic undulation of the track profile), which is also typical of laser welding. This instability results in a vertical deformation of the melt pool close to process conditions which are known to generate keyholes in LPBF [33]. A dynamic melt pool [20] given by fluid instability (Marangoni convection [112]) is due to the comparable size between size of the powder particles and laser spot and dominated by spatially varying absorptivity and vapor recoil [93,113].

Since the physical principles that govern denudation (Marangoni flow and recoil pressure) in single-track scans are the same during the powder bed fusion process, the considerations made on single-track scans can be extended to the complete powder bed fusion process.

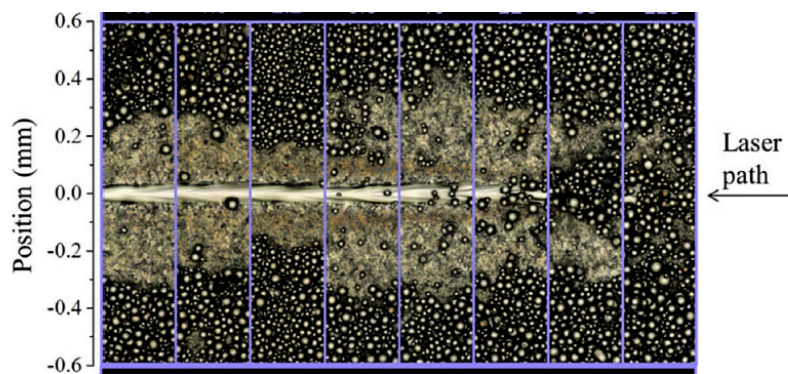


Figure 3. Montage of optical micrographs of a solidified melt track (225 W, 1.4 m/s, Ti-6Al-4V). Adapted from Reference [34] with permission from Elsevier.

3.2. Heat-Affected Powder

During LPBF, it is very common to see very bright ejections (sparks) leaving the laser–powder interaction area; the melt pool undergoes a high degree of superheat, leading to vaporization and material ejection [35,114,115]. Ly et al. [35] reported recently that, while the dominant mechanism of denudation is vapor recoil pressure, the formation of ejections is mostly influenced by vapor-driven entrainment of micro-particles. Since laser powder bed fusion is a very fast process involving high temperatures and very rapid cooling rates, it is of paramount importance to be successful in monitoring the process in terms of laser vapor plume, in order to control its interaction with the metal powder particles, as well as to study the redeposition of the ejections generated during the process itself [116–118].

The heat-affected powder can be classified in terms of its interaction with the heat source (laser) in cold ejections and hot ejections (i.e., the blue circle and red circles in Figure 4, respectively) [35]. The blue ones are particles entrained by the vapor plume and swept on upward and opposite to the laser motion, with high speed; these particles are not properly heated by the laser but only moved. The red ones are still entrained by the plume, but they interact directly with the heat source and are emitted as incandescent particles. It must be pointed out that a portion of the entrained particles contribute to the melt-pool formation.

Given the large difference between the thermal conductivity of pre-alloyed metal powders and the same bulk alloy (100 times higher for 316L stainless steel [119,120]), the heat in the melt pool and its vicinity can exceed the melting temperature, fostering the evaporation phenomenon, whose expansion generates the recoil pressure inside the melt pool. High values of this recoil pressure cause the expulsion of hot ejections [46,121,122]. Ejections are emitted from the laser–powder interaction area with an angle which depends on melt-pool geometry and vapor pressure [123]. The evaporation of the feedstock material under high laser intensity values leads to the formation of a depression and a further

metal vapor plume. The orientation of this plume can be controlled by tuning the above-mentioned process parameters [35]. This effect is clearly evidenced in Figure 5.

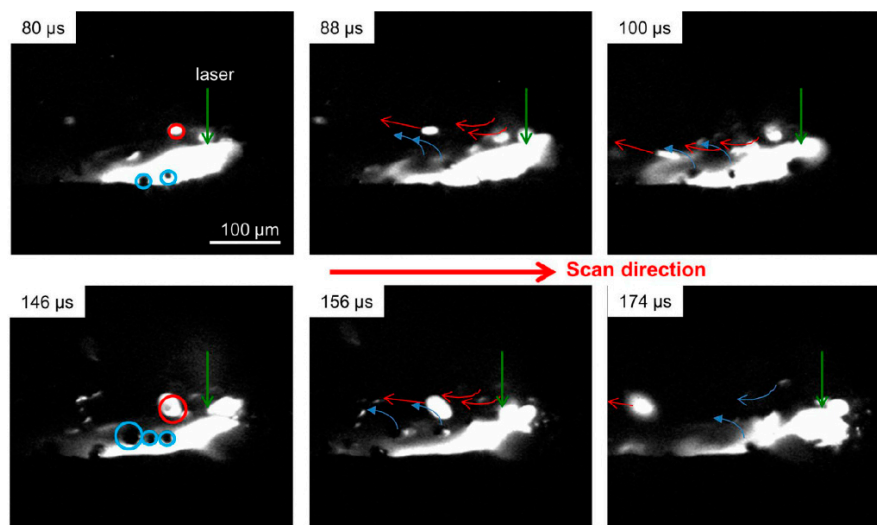


Figure 4. High-resolution images of the melt-pool formation (300 W, 1.5 m/s). Adapted from Reference [35] with permission from Springer Nature.

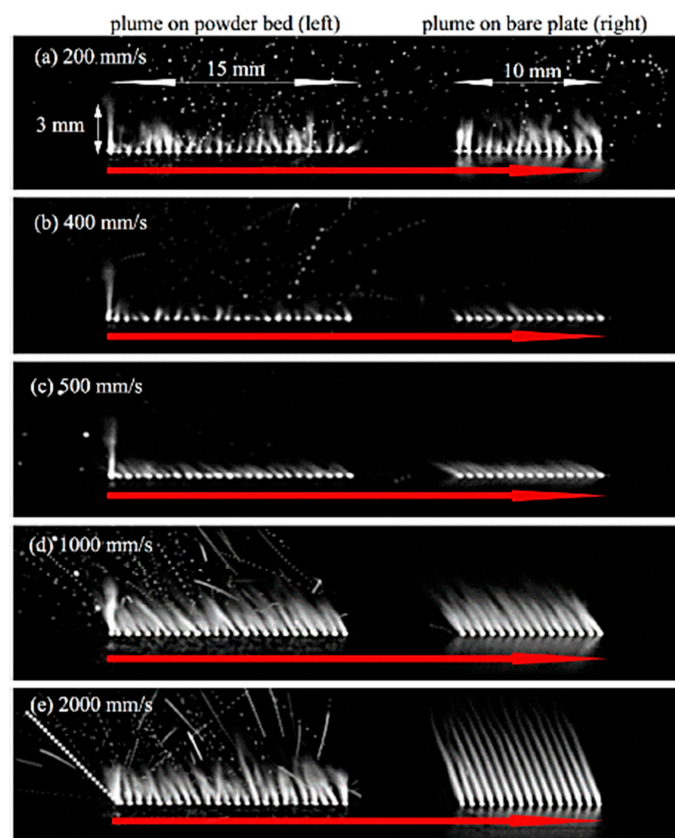


Figure 5. Images of plume and spatter formation under different scan speeds (500 W, 304L stainless steel). Reproduced from Reference [116] with permission from Elsevier.

It is worth noting that ejections can account for up to 35% of the total area of the powder bed being processed, leading to a remarkable loss in material and heat, which must be additionally addressed in order to make the LPBF process more efficient [9].

3.2.1. Spatter

The formation of spatter particles ejected from the laser–powder interaction zone, particularly from the melt-pool area, are known to consistently affect the surface properties of the manufactured parts, as well as to generate inner defects in the sub-surface area, which are difficult to remove without properly tuning the post-processing steps [86,124–127]. Furthermore, very large spatter particles are most likely to generate lack-of-fusion defects in the final parts since, being potentially bigger (larger diameter) than the layer thickness, the process parameters may be not sufficient to fully melt them, and the spreading of the next powder layer could be inefficient [35].

Spatters are typically emitted from the melt pool, where the surface tension generates particles with unique and non-uniform chemical compositions [128]. Looking at all the possible shapes collected in different papers addressing spatter particles, Sutton et al. [101] suggested the following potential classification based on the morphology:

1. Spherical: spatter solidifies without colliding with other particles during flight.
2. Aggregates: spatter collides with neighboring spatter in flight and/or after contacting with the powder bed.
3. Coarse aggregates: multiple spatter particles collide with one another during flight and are completely subsumed.

It is important to point out that spatter particles are mostly spherical, indicating that the cooling rate was low enough to allow surface tension forces to shape the molten material, and it is additionally a property not connected to the nature of the metal powder alloy, as shown by Simonelli et al. [86].

Spatter particles are likely to appear to have a wide size distribution range which depends strongly on the laser power (small power produces small spatters and vice versa [33]), which goes from highly coarse particles (larger than 100 μm), down to particles having diameters within the typical LPBF size distribution (10–45 μm) as demonstrated by several authors [83,101,129,130], which could be the majority of the ejections (even up to 90% [101]) of heat-affected powder and spatter in particular. Therefore, the latter will not be cut out by sieving the metal powder feedstock before reuse and might alter the local chemical composition of the parts to be built, as well as influencing the metal vapor formation, and the further generation and redeposition of condensate material.

A gradual coarsening of reused powders was observed for different metal powder alloys, such as 304L [101], Inconel 718 [19], and Ti64 [79]. Possible reasons behind this behavior could be the size segregation during the spreading process and the fact that smaller particles are more likely to be entrained in the fluid flow induced by the laser–powder interaction [78,101]. Furthermore, it is worth noting that the amount of spatter generated can vary even if process parameters are kept constant, owing to the partial absorption and scattering of the laser radiation given by the metal vapor plume, in a way similar to what happens during laser welding [98,119,121,126,131].

The emission of spatter particles from the laser–powder interaction zone can take place from the front of the melt pool, with a movement similar to a wave front [27,33] as shown by the high-speed photography snapshots in Figure 6.

The depression formed by the action of the laser and the resulting vapor plume generates the elongation of the molten metal which further breaks up into spatter droplets; these are then deflected by the interaction with the laser radiation and fall back on the powder bed.

The emission of spatter particles also takes place from the rear of the melt pool, in a direction which is contrary to the laser direction (Figure 7) [33,132,133]. This highlights that the emission of spatters takes place in different locations of the melt pool and is not specifically driven by the laser motion. Furthermore, Yin et al. [133] pointed out that most of the spatters are ejected backward, while

only a few have a horizontal velocity component along the laser direction. The height, angle, speed, and location of the spatter particles were studied by several authors, who found a strict correlation with the process parameters, mainly scan speed and laser power [33,35,132,133].

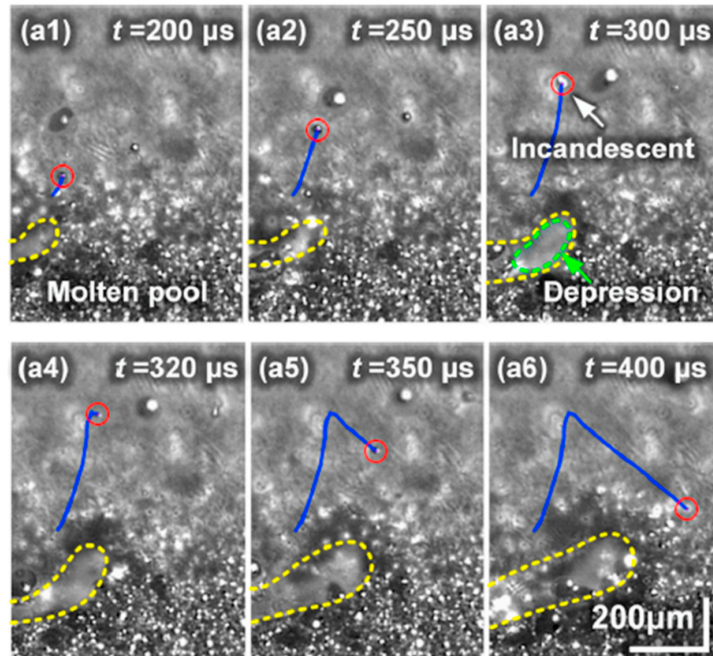


Figure 6. Snapshots of high-speed camera of the forward-ejected spatters, from $t = 200 \mu\text{s}$ to $t = 400 \mu\text{s}$ (from left to right) at a laser power of 1150 W (Inconel 718 powder). Adapted from Reference [132] with permission from Elsevier.

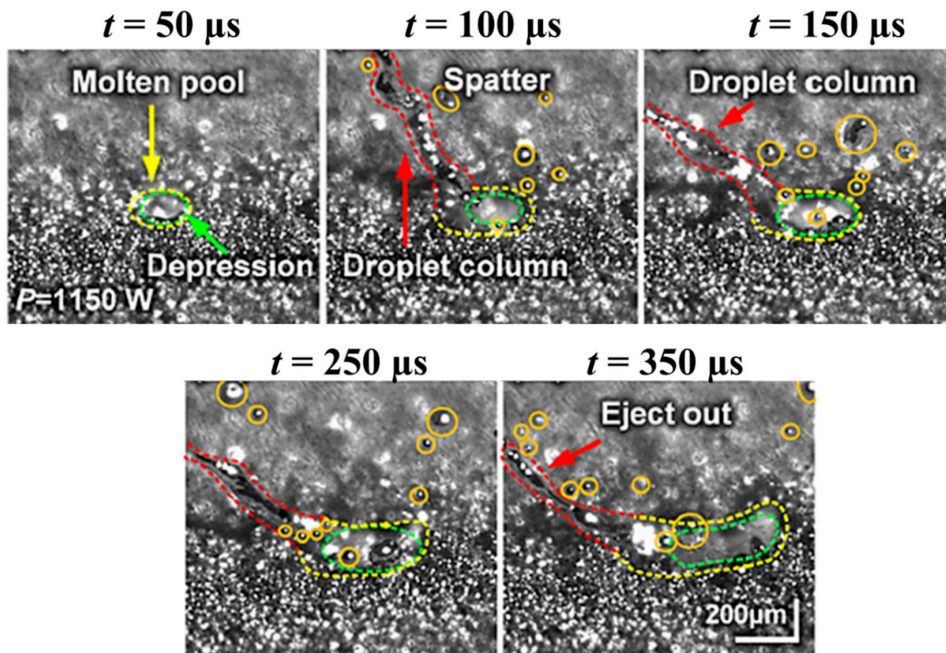


Figure 7. Time-series snapshots of the evolution of the molten pool in LPBF as a function of the laser power. A column of droplets oscillates and eventually breaks up into spatter particles at the rear of the molten pool with a laser power of 1150 W (Inconel 718 powder). Adapted from Reference [133] with permission from Elsevier.

Typically, laser spatter experiences oxidation during flight, and several authors [35,86,101,126,128] reported the formation of a hemispherical oxide island on the surface of laser spatters (Figure 8). Oxidation of metals can be categorized into four stages: induction, nucleation, growth, and coalescence [134]. If there is enough time before the particle completely solidifies, the oxide islands coalesce into the larger oxide islands; however, if the cooling rate of laser spatter is high, the oxide islands are not able to completely combine, hindering the formation of a continuous oxide film and giving rise to the hemispherical shape. Furthermore, through oxygen diffusion in the metal lattice, the oxide layer can penetrate the underlying metal of the particle [122]. The further penetration and growth of the oxide layer will affect the local chemical composition and thermal conductivity. In the case of remelting of these strongly oxidized particles, the resulting melt pool will experience different flow regimes with potential for pore formation and instabilities.

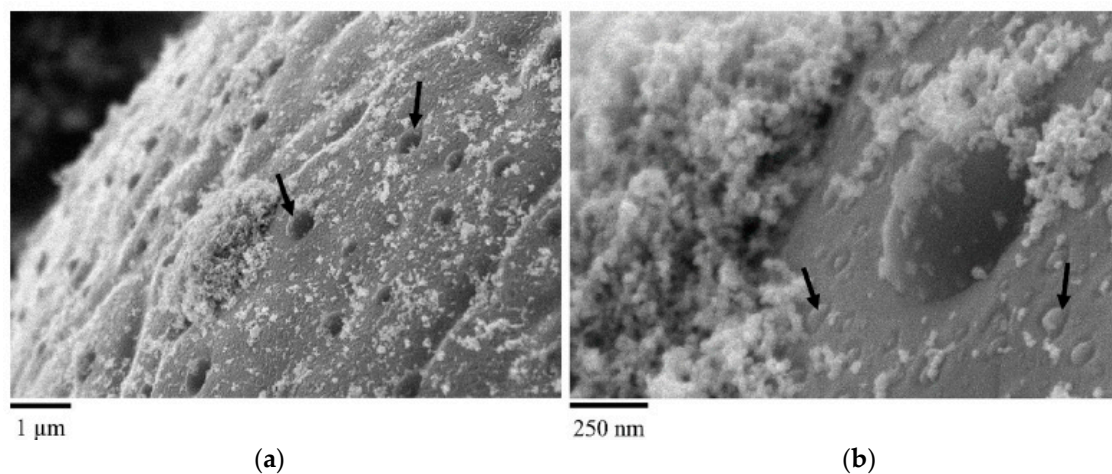


Figure 8. Scanning electron microscopy (SEM) micrographs showing (a) spatter with oxide islands, and (b) higher magnification of the spatter surface. Oxide islands on 304L stainless steel with dimensions ranging from 1 μm to 100 nm (approximately) are depicted with arrows in both images. Adapted from Reference [101] with permission from Elsevier.

Energy-dispersive spectroscopy was also used to identify oxide island patches on the surface of these particles as silicon oxide [101]. These findings agree with work performed by Simonelli et al. [86] who found Mn, Si, and Mg oxides on the surface of laser spatter particles. As mentioned above, when the time of flight is long enough, the surface of the spatter particles can experience strong oxidation, mostly in the case of highly reactive powders (i.e., Ti-6Al-4V) and powders with chemical composition characterized by the high presence of elements with a high oxidation potential (i.e., stainless steels). As a matter of fact, the presence of oxygen and interstitial elements in general (i.e., H, O) on the particles or within the environment of the build chamber (insufficient inert gas flow) can impact the chemical composition of the melt pool and its surface tension, causing unfavorable wetting conditions and affecting the following solidification and densification of the metal part [37,135]. Therefore, depending on the application of the part to be produced (biomedical, aeronautical, structural, or just a prototype), a different level of accuracy concerning the removal of heat-affected particles should be used.

It is also worth noting that, in the case of 316L stainless steel, the interaction of the powder particles with the laser radiation can give rise to ejections with a different phase composition (higher amount of δ ferrite) and to spatter with a high ferrite content (Fe_3O_4 , iron oxide), which could also affect their magnetic behavior and, therefore, their flowability [37,126] (Figure 9).

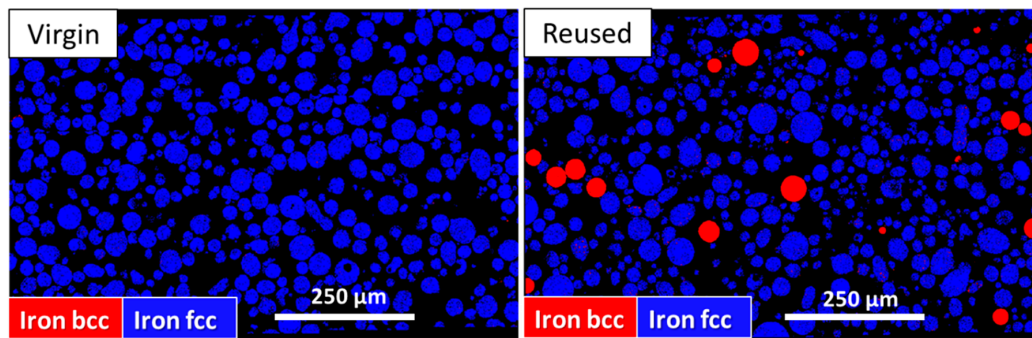


Figure 9. Electron backscatter diffraction (EBSD) phase maps and inverse pole figure montage maps for fcc γ austenite (blue) and bcc δ ferrite (red) regions in virgin and reused powders. Adapted from Reference [37] with permission from Elsevier.

3.2.2. Condensate

One of the side effects of the laser–powder interaction is the formation of a vapor plume due to the evaporation of some (or all) metals of the processed alloy. The environmental conditions inside the build chamber (and the continuous gas flow in particular) lead to the rapid solidification of this vaporized material, which literally condensates inside the chamber. Furthermore, this material can also solidify on the surface of spatter particles and be redeposited on the powder bed, as shown in Figure 10. Despite the presence of condensate in the powder bed already being known, its effects on the mechanical and microstructural properties of final parts is yet to be assessed. It must be pointed out that, if a large amount of condensate is generated and eventually redeposited on the bed together with the ejected (spatter) particles, the surface properties of the powder will change and might influence the flowability of the reused feedstock material [101,135,136].

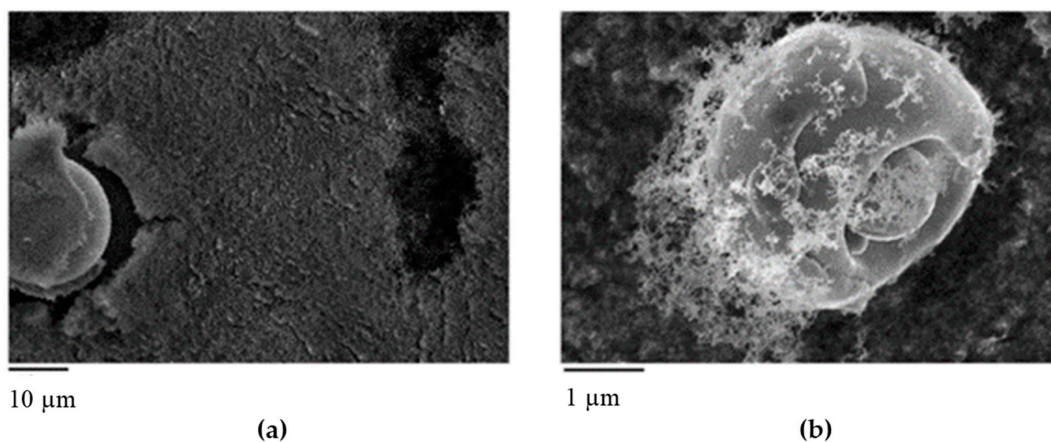


Figure 10. SEM images of condensate: (a) low-magnification micrograph of a sample taken from the chamber wall; (b) condensate deposited on a spatter particle. Reproduced from Reference [101] with permission from Elsevier.

From Figure 10, it is possible to observe that condensate is in the form of nanoparticles since, during the cooling, there is a decrease in metal vapor solubility in the process chamber environment, giving rise to a supersaturated solution with high undercooling, a condition which fosters the formation of nanoparticles [39,97,98,126,137]. These results suggest that the reuse of powders with condensate content should be prevented, but more studies specifically focused on this topic are needed in order to monitor the condensate formation and evolution for different alloys.

All the results reported in the present review paper call for solutions to be found in the scientific community. However, as the LPBF technology is still young and given the ongoing studies worldwide

on the laser–powder interaction, there is still scientific debate on the appropriate research and methodologies to be performed in order to converge to a common solution. In this respect, interesting insight was given by Vermej et al. [138], who addressed the problem of atom redeposition during focused ion beam (FIB) milling. These authors suggested the temporary placement of an optimized polydimethylsiloxane (PDMS) block on the surface of the sample during FIB milling to catch the ejected atoms. Although the solution cannot be applied straightforwardly in LPBF, the use of a similar concept is likely to be of high interest, in addition to being potentially promising. Furthermore, it is known that powder particle interaction during laser beam production of stainless steels can cause a change in the crystal structure and magnetic behavior [37]. Thus, a development of magnetic separators located in the proximity of sieving equipment is believed to enhance the cleanness of the reused powder [139].

4. Conclusions

The present paper gave an overview of the possible side effects of the laser–powder interaction during the LPBF additive manufacturing process. At the end of a LPBF build job, the properties of the powder inside the chamber can be strongly affected by the interaction with the laser radiation and the process environment. Therefore, the reuse of this powder, which is desirable in order to reduce the costs and environmental impact of this manufacturing process, might lead to parts with altered chemical composition and/or mechanical properties. However, the literature showed that the properties of parts built with reused powders are scattered and very different from each other (improved, decreased, or even unaffected), despite referring to similar starting alloys and process parameters.

These results suggest that excessive production of by-products (condensate and spatters) due to the process parameters and their inefficient removal by the gas flow can lead to laser muting (attenuation) and drift, with a local change in the process conditions and consequent variations of microstructural and mechanical properties of the final parts.

A fine-tuning of the process parameters and an extremely accurate gas flow regime seem to be mandatory to make laser powder bed fusion a more reliable process. Furthermore, the adoption of purposely developed systems to remove the generated by-products could speed up this evolution.

Author Contributions: Conceptualization, E.S., S.S. and M.C.; writing—original draft preparation, E.S.; writing—review and editing, E.S., S.S. and M.C. All authors have read and agree to the published version of the manuscript.

Funding: The Grant of Excellence Departments, MIUR-Italy (ARTICOLO 1, COMMI 314-337 LEGGE 232/2016) is gratefully acknowledged.

Conflicts of Interest: The authors declare no conflict of interest.

References

1. Frazier, W.E. Metal Additive Manufacturing: A Review. *J. Mater. Eng. Perform.* **2014**, *23*, 1917–1928. [[CrossRef](#)]
2. Herzog, D.; Seyda, V.; Wycisk, E.; Emmelmann, C. Additive manufacturing of metals. *Acta Mater.* **2016**, *117*, 371–392. [[CrossRef](#)]
3. Du Plessis, A.; Broeckhoven, C. Looking deep into nature: A review of micro-computed tomography in biomimicry. *Acta Biomater.* **2019**, *85*, 27–40. [[CrossRef](#)] [[PubMed](#)]
4. Al-Ketan, O.; Lee, D.-W.; Rowshan, R.; Abu Al-Rub, R.K. Functionally graded and multi-morphology sheet TPMS lattices: Design, manufacturing, and mechanical properties. *J. Mech. Behav. Biomed.* **2020**, *102*, 103520. [[CrossRef](#)] [[PubMed](#)]
5. Großmann, A.; Felger, J.; Frölich, T.; Gosmann, J.; Mittelsted, C. Melt pool controlled laser powder bed fusion for customised low-density lattice structures. *Mater. Des.* **2019**, *181*, 108054. [[CrossRef](#)]
6. Du Plessis, A.; Yadroitsava, I.; Yadroitsev, I. Ti6Al4V lightweight lattice structures manufactured by laser powder bed fusion for load-bearing applications. *Opt. Laser Technol.* **2018**, *108*, 521–528. [[CrossRef](#)]
7. Maloney, K.J.; Fink, K.D.; Schaedler, T.A.; Kolodziejska, J.A.; Jacobsen, A.J.; Roper, C.S. Multifunctional heat exchangers derived from three-dimensional micro-lattice structures. *Int. J. Heat Mass Transf.* **2012**, *55*, 2486–2493. [[CrossRef](#)]

8. Hann, B. Powder reuse and its effects on Laser Based Powder Fusion Additive Manufactured Alloy 718. *SAE Int. J. Aerosp.* **2016**, *9*, 209–213. [[CrossRef](#)]
9. Criales, L.E.; Arisoy, Y.M.; Lane, B.; Moylan, S.; Donmez, A.; Özel, T. Laser powder bed fusion of nickel alloy 625: Experimental investigations of effects of process parameters on melt pool size and shape with spatter analysis. *Int. J. Mach. Tool Manuf.* **2017**, *121*, 22–36. [[CrossRef](#)]
10. Griffith, M.L.; Ensz, M.T.; Puskar, J.D.; Robino, C.V.; Brooks, J.A.; Philliber, J.A.; Smugeresky, J.E.; Hofmeister, W.H. Understanding the microstructure and properties of components fabricated by laser engineered net shaping (LENS). *MRS Proc.* **2000**, *625*, 9. [[CrossRef](#)]
11. Gong, H.; Rafi, K.; Gu, H.; Starr, T.; Stucker, B. Analysis of defect generation in Ti-6Al-4V parts made using powder bed fusion additive manufacturing processes. *Addit. Manuf.* **2014**, *1–4*, 87–98. [[CrossRef](#)]
12. Beese, A.M.; Carroll, B.E. Review of mechanical properties of Ti-6Al-4V made by laser-based additive manufacturing using powder feedstock. *JOM* **2016**, *68*, 724–734. [[CrossRef](#)]
13. Gu, D.D.; Meiners, W.; Wissenbach, K.; Poprawe, R. Laser additive manufacturing of metallic components: Materials, processes and mechanisms. *Int. Mater. Rev.* **2012**, *57*, 133–164. [[CrossRef](#)]
14. Kirka, M.M.; Lee, Y.; Greeley, D.A.; Okello, A.; Goin, M.J.; Pearce, M.T.; Dehoff, R.R. Strategy for texture management in metals additive manufacturing. *JOM* **2017**, *69*, 523–531. [[CrossRef](#)]
15. Cunningham, R.; Narra, S.P.; Montgomery, C.; Beuth, J.; Rollet, A.D. Synchrotron based X-ray microtomography characterization of the effect of processing variables on porosity formation in laser power-bed additive manufacturing of Ti-6Al-4V. *JOM* **2017**, *69*, 479–484. [[CrossRef](#)]
16. King, W.E.; Anderson, A.T.; Ferencz, R.M.; Hodge, N.E.; Kamath, C.; Khairallah, S.A.; Rubenchik, A.M. Laser powder bed fusion additive manufacturing of metals; physics, computational, and materials challenges. *App. Phys. Rev.* **2015**, *2*, 041304. [[CrossRef](#)]
17. Anderson, I.E.; White, E.M.H.; Dehoff, R. Feedstock powder processing research needs for additive manufacturing development. *Curr. Opin. Solid State Mater. Sci.* **2018**, *22*, 8–15. [[CrossRef](#)]
18. DebRoy, T.; Wei, H.L.; Zuback, J.S.; Mukherjee, T.; Elmer, J.W.; Milewski, J.O.; Beese, A.M.; Wilson-Heid, A.; Ded, A.; Zhang, W. Additive manufacturing of metallic components—Process, structure and properties. *Prog. Mater. Sci.* **2018**, *92*, 112–224. [[CrossRef](#)]
19. Ardila, L.C.; Garciandia, F.; González-Díaz, J.B.; Álvarez, P.; Echeverria, A.; Petite, M.M.; Deffley, R.; Ochoa, J. Effect of IN718 recycled powder reuse on properties of parts manufactured by means of selective laser melting. *Phys. Procedia* **2014**, *56*, 99–107. [[CrossRef](#)]
20. Guo, Q.; Zhao, C.; Qu, M.; Xiong, L.; Escano, L.I.; Hojjatzadeh, S.M.H.; Parab, N.D.; Fezzaa, K.; Everhart, W.; Sun, T.; et al. In-situ characterization and quantification of melt pool variation under constant input energy density in laser powder bed fusion additive manufacturing process. *Addit. Manuf.* **2019**, *28*, 600–609. [[CrossRef](#)]
21. Fabbro, R. Melt pool and keyhole behaviour analysis for deep penetration laser welding. *J. Phys. D Appl. Phys.* **2010**, *43*, 445501. [[CrossRef](#)]
22. Gladush, G.G.; Smurov, I. *Physics of Laser Materials Processing: Theory and Experiment*; Springer: New York, NY, USA, 2011.
23. Vock, S.; Klöden, B.; Kirchner, A.; Weißgärber, T.; Kieback, B. Powders for powder bed fusion: A review. *Prog. Addit. Manuf.* **2019**, *4*, 383–397. [[CrossRef](#)]
24. Niu, X.; Singh, S.; Garg, A.; Singh, H.; Panda, B.; Peng, X.; Zhang, Q. Review of materials used in laser-aided additive manufacturing processes to produce metallic products. *Front. Mech. Eng.* **2019**, *14*, 282–298. [[CrossRef](#)]
25. Samant, R.; Lewis, B. *Metal Powder Recycling and Reconditioning in Additive Manufacturing*; EWI: Columbus, OH, USA, 2017.
26. Thompson, S.M.; Bian, L.; Shamsaei, N.; Yadollahi, A. An overview of Direct Laser Deposition for additive manufacturing; Part I: Transport phenomena, modeling and diagnostics. *Addit. Manuf.* **2015**, *8*, 36–62. [[CrossRef](#)]
27. Khairallah, S.A.; Anderson, A.T.; Rubenchik, A.M.; King, W.E. Laser powder-bed fusion additive manufacturing: Physics of complex melt flow and formation mechanisms of pores, spatter, and denudation zones. *Acta Mater.* **2016**, *108*, 36–45. [[CrossRef](#)]
28. Lutter-Günther, M.; Bröker, M.; Mayer, T.; Lizak, S.; Seidel, C.; Reinhart, G. Spatter formation during laser beam melting of AlSi10Mg and effects on powder quality. *Procedia CIRP* **2018**, *74*, 33–38. [[CrossRef](#)]

29. ASTM F2924-14, *Standard Specification for Additive Manufacturing Titanium-6 Aluminum-4 Vanadium with Powder Bed Fusion*; ASTM International: West Conshohocken, PA, USA, 2014.
30. Denti, L.; Sola, A.; Defanti, S.; Sciancalepore, C.; Bondioli, F. Effect of Powder Recycling in Laser-based Powder Bed Fusion of Ti-6Al-4V. *Manuf. Technol.* **2019**, *19*, 190–196. [[CrossRef](#)]
31. Markl, M.; Korner, C. Multiscale modeling of powder bed-based additive manufacturing. *Ann. Rev. Mater. Res.* **2016**, *46*, 93–123. [[CrossRef](#)]
32. Scipioni Bertoli, U.; Guss, G.; Wu, S.; Matthews, M.J.; Schoenung, J.M. In-situ characterization of laser-powder interaction and cooling rates through high-speed imaging of powder bed fusion additive manufacturing. *Mater. Des.* **2017**, *135*, 385–396. [[CrossRef](#)]
33. Gunenthiram, V.; Peyre, P.; Schneider, M.; Dal, M.; Coste, F.; Fabbro, R. Analysis of laser–melt pool–powder bed interaction during the selective laser melting of a stainless steel. *J. Laser Appl.* **2017**, *29*, 022303. [[CrossRef](#)]
34. Matthews, M.J.; Guss, G.; Khairallah, S.A.; Rubenchik, A.M.; Depond, P.J.; King, W.E. Denudation of metal powder layers in laser powder bed fusion processes. *Acta Mater.* **2016**, *114*, 33–42. [[CrossRef](#)]
35. Ly, S.; Rubenchik, A.M.; Khairallah, S.A.; Guss, G.; Matthews, M.J. Metal vapor microjet controls material redistribution in laser powder bed fusion additive manufacturing. *Sci. Rep.* **2017**, *7*, 4085. [[CrossRef](#)] [[PubMed](#)]
36. Simonelli, M.; Tse, Y.Y.; Tuck, C. Effect of the build orientation on the mechanical properties and fracture modes of SLM Ti-6Al-4V. *Mater. Sci. Eng. A* **2014**, *616*, 1–11. [[CrossRef](#)]
37. Heiden, M.J.; Deibler, L.A.; Rodelas, J.M.; Koepke, J.R.; Tung, D.J.; Saiz, D.J.; Jared, B.H. Evolution of 316L stainless steel feedstock due to laser powder bed fusion process. *Addit. Manuf.* **2019**, *25*, 84–103. [[CrossRef](#)]
38. Jamshidinia, M.; Kovacevic, R. The influence of heat accumulation on the surface roughness in powder-bed additive manufacturing. *Surf. Topogr. Metrol. Prop.* **2015**, *3*, 014003. [[CrossRef](#)]
39. Ferrar, B.; Mullen, L.; Jones, E.; Stamp, R.; Sutcliffe, C.J. Gasflow effects on selective laser melting (SLM) manufacturing performance. *J. Mater. Process. Technol.* **2012**, *212*, 355–364. [[CrossRef](#)]
40. Ahmed, F.; Ali, U.; Sarker, D.; Marzbanrad, E.; Choi, K.; Mahmoodkhani, Y.; Toyserkani, E. Study of powder recycling and its effect on printed parts during laser powder-bed fusion of 17-4 PH stainless steel. *J. Mater. Process. Technol.* **2020**, *278*, 116522. [[CrossRef](#)]
41. Fischer, P.; Romano, V.; Weber, H.P.; Karapatis, N.P.; Boillat, E.; Glardon, R. Sintering of commercially pure titanium powder with a Nd:YAG laser source. *Acta Mater.* **2003**, *51*, 1651–1662. [[CrossRef](#)]
42. Simchi, A. Direct laser sintering of metal powders: Mechanism, kinetics and microstructural features. *Mater. Sci. Eng. A* **2006**, *428*, 148–158. [[CrossRef](#)]
43. Von Allmen, M.F.; Blatter, A. *Laser-Beam Interactions with Materials*; Springer: Berlin, Germany, 1994.
44. Slavin, A.J.; Arcas, V.; Greenhalgh, C.A.; Irvine, E.R.; Marshall, D.B. Theoretical model for the thermal conductivity of a packed bed of solid spheroids in the presence of a static gas with no adjustable parameters except pressure and temperature. *Int. J. Heat Mass Transf.* **2002**, *45*, 4151–4161. [[CrossRef](#)]
45. Starke, E.J.; Fine, M.E. *Rapidly Solidified Powder Aluminum Alloys*; ASTM: West Conshohocken, PA, USA, 1986.
46. Kruth, J.P.; Froyen, L.; Van Vaerenbergh, J.; Mercelis, P.; Rombouts, M.; Lauwers, B. Selective laser melting of iron-based powder. *J. Mater. Process. Technol.* **2004**, *149*, 616–622. [[CrossRef](#)]
47. Hebert, R.J. Viewpoint: Metallurgical aspects of powder bed metal additive manufacturing. *J. Mater. Sci.* **2016**, *51*, 1165–1175. [[CrossRef](#)]
48. Yadroitsev, I.; Gusarov, A.; Yadroitsava, I.; Smurov, I. Single track formation in selective laser melting of metal powders. *J. Mater. Process. Technol.* **2010**, *210*, 1624–1631. [[CrossRef](#)]
49. Aversa, A.; Moshiri, M.; Librera, E.; Hadi, M.; Marchese, G.; Manfredi, D.; Lorusso, M.; Calignano, F.; Biamino, S.; Lombardi, M.; et al. Single scan track analyses on aluminium based powders. *J. Mater. Process. Technol.* **2018**, *255*, 17–25. [[CrossRef](#)]
50. Shrestha, S.; Chou, K. Single track scanning experiment in laser powder bed fusion process. *Procedia Manuf.* **2018**, *26*, 857–864. [[CrossRef](#)]
51. Makoana, N.W.; Yadroitsava, I.; Möller, H.; Yadroitsev, I. Characterization of 17-4PH Single Tracks Produced at Different Parametric Conditions towards Increased Productivity of LPBF Systems—The Effect of Laser Power and Spot Size Upscaling. *Metals* **2018**, *8*, 475. [[CrossRef](#)]
52. Simchi, A. The role of particle size on the laser sintering of iron powder. *Metall. Mater. Trans. B* **2004**, *35*, 937–948. [[CrossRef](#)]

53. Yadroitsev, I.; Bertrand, P.; Smurov, I. Parametric analysis of selective laser melting technology. *Appl. Surf. Sci.* **2007**, *253*, 8064–8069. [[CrossRef](#)]
54. Mumtaz, K.A.; Erasenthiran, P.; Hopkinson, N. High density selective laser melting of Waspaloy®. *J. Mater. Process. Technol.* **2008**, *195*, 77–87. [[CrossRef](#)]
55. Bricín, D.; Kříž, A. Assessment of Usability of WC-Co Powder Mixtures for SLM. *Manuf. Technol.* **2018**, *18*, 719–726.
56. Zhao, X.M.; Chen, J.; Lin, X.; Huang, W.D. Study on microstructure and mechanical properties of laser rapid forming Inconel 718. *Mater. Sci. Eng. A* **2008**, *478*, 119–124. [[CrossRef](#)]
57. Sames, W.J.; List, F.A.; Pannala, S.; Dehoff, R.R.; Babu, S.S. The metallurgy and processing science of metal additive manufacturing. *Int. Mater. Rev.* **2016**, *61*, 315–360. [[CrossRef](#)]
58. Slotwinski, J.A.; Garboczi, E.J.; Stutzman, P.E.; Ferraris, C.F.; Watson, S.S.; Peltz, M.A. Characterization of metal powders used for additive manufacturing. *J. Res. Natl. Inst. Stand.* **2014**, *119*, 460–493. [[CrossRef](#)] [[PubMed](#)]
59. Santomaso, A.; Lazzaro, P.; Canu, P. Powder flowability and density ratios: The impact of granules packing. *Chem. Eng. Sci.* **2003**, *58*, 2857–2874. [[CrossRef](#)]
60. Gatto, A.; Bassoli, E.; Denti, L. Repercussions of powder contamination on the fatigue life of additive manufactured maraging steel. *Addit. Manuf.* **2018**, *24*, 13–19. [[CrossRef](#)]
61. Seifi, M.; Salem, A.; Beuth, J.; Harrysson, O.; Lewandowski, J.J. Overview of Materials Qualification Needs for Metal Additive Manufacturing. *JOM* **2016**, *68*, 747–764. [[CrossRef](#)]
62. Dawes, J.; Bowerman, R.; Trepleton, R. Introduction to the Additive Manufacturing Powder Metallurgy Supply Chain. *Johnson Matthey Technol. Rev.* **2015**, *59*, 243–256. [[CrossRef](#)]
63. Chen, G.; Zhao, S.Y.; Tan, P.; Wang, J.; Xiang, C.S.; Tang, H.P. A comparative study of Ti-6Al-4V powders for additive manufacturing by gas atomization, plasma rotating electrode process and plasma atomization. *Powder Technol.* **2018**, *333*, 38–46. [[CrossRef](#)]
64. Mostafaei, A.; Hilla, C.; Stevens, E.L.; Nandwana, P.; Elliott, A.M.; Chmielus, M. Comparison of characterization methods for differently atomized nickel-based alloy 625 powders. *Powder Technol.* **2018**, *333*, 180–192. [[CrossRef](#)]
65. Goncharov, I.S.; Razumov, N.G.; Silin, A.O.; Ozerskoi, N.E.; Shamshurin, A.I.; Kim, A.; Wang, Q.S.; Popovich, A.A. Synthesis of Nb-based powder alloy by mechanical alloying and plasma spheroidization processes for additive manufacturing. *Mater. Lett.* **2019**, *245*, 188–191. [[CrossRef](#)]
66. Si, C.; Tang, X.; Zhang, X.; Wang, J.; Wu, W. Characteristics of 7055Al alloy powders manufactured by gas-solid two-phase atomization: A comparison with gas atomization process. *Mater. Des.* **2017**, *118*, 66–74. [[CrossRef](#)]
67. Garboczi, E.J.; Hrabe, N. Particle shape and size analysis for metal powders used for additive manufacturing: Technique description and application to two gas-atomized and plasma-atomized Ti64 powders. *Addit. Manuf.* **2020**, *31*, 100965. [[CrossRef](#)]
68. Anderson, I.E.; Terpstra, R.L. Progress toward gas atomization processing with increased uniformity and control. *Mater. Sci. Eng. A* **2002**, *326*, 101–109. [[CrossRef](#)]
69. Bourdeau, R.G. Rotary Atomizing Process. U.S. Patent No. 4,415,511, 15 November 1983.
70. Seki, Y.; Okamoto, S.; Takigawa, H.; Kawai, N. Effect of atomization variables on powder characteristics in the high-pressure water atomization process. *Met. Powder. Rep.* **1990**, *45*, 38–40. [[CrossRef](#)]
71. Champagne, B.; Angers, R. PREP (Rotating Electrode Process) atomization mechanisms. *Powder Metall. Int.* **1984**, *16*, 125–128.
72. Ozols, A.; Sirkin, H.R.; Vicente, E.E. Segregation in Stellite powders produced by the plasma rotating electrode process. *Mater. Sci. Eng. A* **1999**, *262*, 64–69. [[CrossRef](#)]
73. Wei, W.-H.; Wang, L.-Z.; Chen, T.; Duan, X.-M.; Li, W. Study on the flow properties of Ti-6Al-4V powders prepared by radio-frequency plasma spheroidization. *Adv. Powder Technol.* **2017**, *28*, 2431–2437. [[CrossRef](#)]
74. Ustundag, M.; Varol, R. Comparison of a commercial powder and a powder produced from Ti-6Al-4V chips and their effects on compacts sintered by the sinter-HIP method. *Int. J. Min. Met. Mater.* **2019**, *26*, 878–888. [[CrossRef](#)]
75. Soufiani, A.M.; Karimzadeh, F.; Enayati, M.H.; Soufiani, A.M. The effect of type of atmospheric gas on milling behavior of nanostructured Ti6Al4V alloy. *Adv. Powder Technol.* **2012**, *23*, 264–267. [[CrossRef](#)]

76. Canakci, A.; Varol, T. A novel method for the production of metal powders without conventional atomization process. *J. Clean. Prod.* **2015**, *99*, 312–319. [[CrossRef](#)]
77. Lutter-Günther, M.; Gebbe, C.; Kamps, T.; Seidel, C.; Reinhart, G. Powder recycling in laser beam melting: Strategies, consumption modeling and influence on resource efficiency. *Prod. Eng. Res. Dev.* **2018**, *12*, 377–389. [[CrossRef](#)]
78. Strondl, A.; Lyckfeldt, O.; Brodin, H.; Ackelid, U. Characterization and control of powder properties for additive manufacturing. *JOM* **2015**, *67*, 549–554. [[CrossRef](#)]
79. Seyda, V.; Kaufmann, N.; Emmelmann, C. Investigation of aging processes of Ti-6Al-4 V powder material in laser melting. *Phys. Proc.* **2012**, *39*, 425–431. [[CrossRef](#)]
80. Maamoun, A.H.; Elbestawi, M.; Dosbaeva, G.K.; Veldhuis, S.C. Thermal post-processing of AlSi10Mg parts produced by selective laser melting using recycled powder. *Addit. Manuf.* **2018**, *21*, 234–247. [[CrossRef](#)]
81. Del Re, F.; Contaldi, V.; Astarita, A.; Palumbo, B.; Squillace, A.; Corrado, P.; Di Petta, P. Statistical approach for assessing the effect of powder reuse on the final quality of AlSi10Mg parts produced by laser powder bed fusion additive manufacturing. *Int. J. Adv. Manuf. Technol.* **2018**, *97*, 2231–2240. [[CrossRef](#)]
82. Cordova, L.; Campos, M.; Tinga, T. Revealing the Effects of Powder Reuse for Selective Laser Melting by Powder Characterization. *JOM* **2019**, *71*, 1062–1072. [[CrossRef](#)]
83. Asgari, H.; Baxter, C.; Hosseinkhani, K.; Mohammadi, M. On microstructure and mechanical properties of additively manufactured AlSi10Mg_200C using recycled powder. *Mater. Sci. Eng. A* **2017**, *707*, 148–158. [[CrossRef](#)]
84. Galicki, D.; List, F.; Babu, S.S.; Plotkowski, A.; Meyer, H.M.; Seals, R.; Hayes, C. Localized Changes of Stainless Steel Powder Characteristics During Selective Laser Melting Additive Manufacturing. *Metall. Mater. Trans. A* **2019**, *50*, 1582–1605. [[CrossRef](#)]
85. Quintana, O.A.; Alvarez, J.; Mcmillan, R.; Tong, W.; Tomonto, C. Effects of Reusing Ti-6Al-4V Powder in a Selective Laser Melting Additive System Operated in an Industrial Setting. *JOM* **2018**, *70*, 1863–1869. [[CrossRef](#)]
86. Simonelli, M.; Tuck, C.; Aboulkhair, N.T.; Maskery, I.; Ashcroft, I.; Wildman, R.D.; Hague, R. A study on the laser spatter and the oxidation reactions during selective laser melting of 316L stainless steel, Al-Si10-Mg, and Ti-6Al-4V. *Metall. Mater. Trans. A* **2015**, *46*, 3842–3851. [[CrossRef](#)]
87. Carrion, P.E.; Soltani-Tehrani, A.; Phan, N.; Shamsaei, N. Powder Recycling Effects on the Tensile and Fatigue Behavior of Additively Manufactured Ti-6Al-4V Parts. *JOM* **2019**, *71*, 963–973. [[CrossRef](#)]
88. Hadadzadeh, A.; Baxter, C.; Shalchi Amirkhiz, B.; Mohammadi, M. Strengthening mechanisms in direct metal laser sintered AlSi10Mg: Comparison between virgin and recycled powders. *Addit. Manuf.* **2018**, *23*, 108–120. [[CrossRef](#)]
89. Ali, U.; Esmailizadeh, R.; Ahmed, F.; Sarker, D.; Muhammad, W.; Keshavarzkermani, A.; Mahmoodkhani, Y.; Marzbanrad, E.; Toyserkani, E. Identification and characterization of spatter particles and their effect on surface roughness, density and mechanical response of 17-4PH stainless steel laser powder-bed fusion parts. *Mater. Sci. Eng. A* **2019**, *756*, 98–107. [[CrossRef](#)]
90. Fischer, P.; Karapatis, N.; Romano, V.; Glardon, R.; Weber, H.P. A model for the interaction of near-infrared laser pulses with metal powders in selective laser sintering. *Appl. Phys. Mater. Sci. Process* **2002**, *74*, 467–474. [[CrossRef](#)]
91. Tapia, G.; Khairallah, S.A.; Matthews, M.J.; King, W.E.; Elwany, A. Gaussian process based surrogate modeling framework for process planning in laser powder-bed fusion additive manufacturing of 316L stainless steel. *Int. J. Adv. Manuf. Technol.* **2018**, *94*, 3591–3603. [[CrossRef](#)]
92. Metelkova, J.; Kinds, Y.; Kempen, K.; Formanoir, C.; Witvrouw, A.; van Hooreweder, B. On the influence of laser defocusing in selective laser melting of 316L. *Addit. Manuf.* **2018**, *3*, 161–169. [[CrossRef](#)]
93. Kaplan, A.F.H. Modelling the primary impact of an Yb: Fibre laser beam profile on the keyhole front. *Phys. Procedia* **2011**, *12*, 627–637. [[CrossRef](#)]
94. Tenbrock, C.; Fischer, F.G.; Wissenbach, K.; Schleifenbaum, J.H.; Wagenblast, P.; Meiners, W.; Wagner, J. Influence of keyhole and conduction mode melting for top-hat shaped beam profiles in laser powder bed fusion. *J. Mater. Process. Technol.* **2020**, *278*, 116514. [[CrossRef](#)]
95. Nie, B.; Yang, L.; Huang, H.; Bai, S.; Wan, P.; Liu, J. Femtosecond laser additive manufacturing of iron and tungsten parts. *Appl. Phys. A* **2015**, *119*, 1075–1080. [[CrossRef](#)]

96. Ngo, T.D.; Kashani, A.; Imbalzano, G.; Nguyen, K.T.Q.; Hui, D. Additive manufacturing (3D printing): A review of materials, methods, applications and challenges. *Compos. Part B* **2018**, *143*, 172–196. [[CrossRef](#)]
97. Ladewig, A.; Schlick, G.; Fisser, M.; Schulze, V.; Glatzel, U. Influence of the shielding gas flow on the removal of process by-products in the selective laser melting process. *Addit. Manuf.* **2016**, *10*, 1–9. [[CrossRef](#)]
98. Shcheglov, P.Y.; Gumenyuk, A.V.; Gornushkin, I.B.; Rethmeier, R.; Petrovskiy, V.N. Vapor-plasma plume investigation during high-power fiber laser welding. *Laser Phys.* **2012**, *23*, 016001. [[CrossRef](#)]
99. Greses, J.; Hilton, P.A.; Barlow, C.Y.; Steen, W.M. Plume attenuation under high power Nd:yttrium-aluminium-garnet laser welding. *J. Laser Appl.* **2004**, *16*, 9. [[CrossRef](#)]
100. Grünberger, T.; Domröse, R. Identification of process phenomena by optical in-process monitoring. *Laser Technik J.* **2015**, *1*, 45–48. [[CrossRef](#)]
101. Sutton, A.T.; Kriewall, C.S.; Leu, M.C.; Newkirk, J.W.; Brown, B. Characterization of laser spatter and condensate generated during the selective laser melting of 304L stainless steel powder. *Addit. Manuf.* **2020**, *31*, 100904. [[CrossRef](#)]
102. Puzon, C.; Forêt, P.; Hryha, E.; Arunprasad, T. Effect of helium – argon mixtures as laser – powder bed fusion processing atmospheres on the properties of the built Ti-6Al-4V parts. In Proceedings of the WorldPM2018 Congress, Beijing, China, 16–20 September 2018; pp. 1633–1639.
103. Puzon, C.; Forêt, P.; Hryha, E.; Arunprasad, T.; Nyborg, L. Argon-helium mixtures as Laser-Powder Bed Fusion atmospheres: Towards increased build rate of Ti-6Al-4V. *J. Mater. Process. Technol.* **2020**, *279*, 116555. [[CrossRef](#)]
104. Campanelli, S.L.; Casalino, G.; Contuzzi, N.; Angelastro, A.; Ludovico, A.D. Analysis of the molten/solidified zone in selective laser melted parts. *SPIE LASE* **2014**, *8963*, 896311.
105. Farshidianfar, M.H.; Khajepour, A.; Gerlich, A.P. Effect of real-time cooling rate on microstructure in Laser Additive Manufacturing. *J. Mater. Process. Technol.* **2016**, *231*, 468–478. [[CrossRef](#)]
106. Yadroitsev, I.; Yadroitsava, I.; Bertrand, P.; Smurov, I. Factor analysis of selective laser melting process parameters and geometrical characteristics of synthesized single tracks. *Rapid Prototyping J.* **2012**, *18*, 201–208. [[CrossRef](#)]
107. Fabbro, R. Scaling laws for the laser welding process in keyhole mode. *J. Mater. Process. Technol.* **2019**, *264*, 346–351. [[CrossRef](#)]
108. Liu, Y.; Zhang, J.; Pang, Z.; Wu, W. Investigation into the influence of laser energy input on selective laser melted thin-walled parts by response surface method. *Opt. Lasers Eng.* **2018**, *103*, 34–45. [[CrossRef](#)]
109. Do, D.K.; Li, P. The effect of laser energy input on the microstructure, physical and mechanical properties of Ti-6Al-4V alloys by selective laser melting. *Virtual Phys. Prototyp.* **2016**, *11*, 41–47. [[CrossRef](#)]
110. Cherry, J.; Davies, H.; Mehmood, S.; Lavery, N.; Brown, S.; Sienz, J. Investigation into the effect of process parameters on microstructural and physical properties of 316L stainless steel parts by selective laser melting. *Int. J. Adv. Manuf. Technol.* **2015**, *76*, 869–879. [[CrossRef](#)]
111. Anthony, T.R.; Cline, H.E. Surface rippling induced by surface-tension gradients during laser surface melting and alloying. *J. Appl. Phys.* **1977**, *48*, 3888–3894. [[CrossRef](#)]
112. Wang, D.; Wu, S.; Fu, F.; Mai, S.; Yang, Y.; Liu, Y.; Song, C. Mechanisms and characteristics of spatter generation in SLM processing and its effect on the properties. *Mater. Des.* **2017**, *117*, 121–130. [[CrossRef](#)]
113. Bauerle, D. *Laser Processing and Chemistry*; Springer: Berlin, Germany, 2011.
114. Zhang, M.J.; Chen, G.Y.; Zhou, Y.; Li, S.C.; Deng, H. Observation of spatter formation mechanisms in high-power fiber laser welding of thick plate. *Appl. Surf. Sci.* **2013**, *280*, 868–875. [[CrossRef](#)]
115. Kawahito, Y.; Mizutani, M.; Katayama, S. High quality welding of stainless steel with 10 kW high power fibre laser. *Sci. Technol. Weld. Join.* **2009**, *14*, 288–294. [[CrossRef](#)]
116. Zheng, H.; Li, H.; Lang, L.; Gong, S.; Ge, Y. Effects of scan speed on vapor plume behavior and spatter generation in laser powder bed fusion additive manufacturing. *J. Manuf. Process.* **2018**, *36*, 60–67. [[CrossRef](#)]
117. Ye, D.; Ying Hsi Fuh, J.; Zhang, Y.; Soon Hong, G.; Zhu, K. In situ monitoring of selective laser melting using plume and spatter signatures by deep belief networks. *ISA Trans.* **2018**, *81*, 96–104. [[CrossRef](#)]
118. Ozel, T.; Shaurya, A.; Altay, A.; Yang, L. Process monitoring of meltpool and spatter for temporal-spatial modeling of laser powder bed fusion process. *Procedia CIRP* **2018**, *74*, 102–106. [[CrossRef](#)]
119. Rombouts, M.; Kruth, J.P.; Froyen, L. Fundamentals of selective laser melting of alloyed steel powders. *CIRP Ann. Manuf. Technol.* **2006**, *55*, 187–192. [[CrossRef](#)]

120. Rombouts, M.; Froyen, L.; Gusarov, A.V.; Bentefour, E.H.; Glorieux, C. Photopyroelectric measurement of thermal conductivity of metallic powders. *J. Appl. Phys.* **2005**, *97*, 024905. [[CrossRef](#)]
121. Fabbro, R.; Slimani, S.; Doudet, I.; Coste, F.; Brian, F. Experimental study of the dynamical coupling between the induced vapour plume and the melt pool for Nd-YAG CW laser welding. *J. Phys. D Appl. Phys.* **2006**, *39*, 394–400. [[CrossRef](#)]
122. Gasper, A.N.D.; Szost, B.; Wang, X.; Johns, D.; Sharma, S.; Clare, A.T.; Ashcroft, I.A. Spatter and oxide formation in laser powder bed fusion of Inconel 718. *Addit. Manuf.* **2018**, *24*, 446–456. [[CrossRef](#)]
123. King, W.E.; Barth, H.D.; Castillo, V.M.; Gallegos, G.F.; Gibbs, J.W.; Hahn, D.E.; Kamath, C.; Rubenchik, A.M. Observation of keyhole-mode laser melting in laser powder-bed fusion additive manufacturing. *J. Mater. Process. Technol.* **2014**, *214*, 2915–2925. [[CrossRef](#)]
124. Nasab, M.H.; Gastaldi, D.; Lecis, N.F.; Vedani, M. On morphological surface features of the parts printed by selective laser melting (SLM). *Addit. Manuf.* **2018**, *24*, 373–377. [[CrossRef](#)]
125. Esmailzadeh, R.; Ali, U.; Keshavarzkermani, A.; Mahmoodkhani, Y.; Marzbanrad, E.; Toyserkani, E. On the effect of spatter particles distribution on the quality of Hastelloy X parts made by laser powder-bed fusion additive manufacturing. *J. Manuf. Process.* **2019**, *37*, 11–20. [[CrossRef](#)]
126. Liu, Y.; Yang, Y.; Mai, S.; Wang, D.; Song, C. Investigation into spatter behavior during selective laser melting of AISI 316L stainless steel powder. *Mater. Des.* **2015**, *87*, 797–806. [[CrossRef](#)]
127. Nasab, M.H.; Giussani, A.; Gastaldi, D.; Tirelli, V.; Vedani, M. Effect of Surface and Subsurface Defects on Fatigue Behavior of AlSi10Mg Alloy Processed by Laser Powder Bed Fusion (L-PBF). *Metals* **2019**, *9*, 1063. [[CrossRef](#)]
128. Taheri Andani, M.; Dehghani, R.; Karamooz-Ravari, M.R.; Mirzaeifar, R.; Ni, J. Spatter formation in selective laser melting process using multi-laser technology. *Mater. Des.* **2017**, *131*, 460–469. [[CrossRef](#)]
129. Sutton, A.T.; Kriewall, C.S.; Leu, M.; Newkirk, J. Characterization of heat-affected powder generated during the selective laser melting of 304L stainless steel powder. In Proceedings of the Solid Freeform Conference, Austin, TX, USA, 7–9 August 2017.
130. Sartin, B.; Pond, T.; Griffith, B.; Everhart, W.; Elder, L.; Wenski, E.; Cook, C.; Wieliczka, D.; King, W.E.; Rubenchik, A.M.; et al. 316L powder reuse for metal additive manufacturing. *Solid Freeform Fabr. Symp. Proc.* **2017**, *2017*, 351–364.
131. Shcheglov, P.Y.; Uspenskiy, S.A.; Gumenyuk, A.V.; Petrovskiy, V.N.; Rethmeier, M.; Yermachenko, V.M. Plume attenuation of laser radiation during high power fiber laser welding. *Laser Phys. Lett.* **2011**, *8*, 475–480. [[CrossRef](#)]
132. Yin, J.; Wang, D.; Yang, L.; Wei, H.; Dong, P.; Ke, L.; Wang, G.; Zhu, H.; Zeng, X. Correlation between forming quality and spatter dynamics in laser powder bed fusion. *Addit. Manuf.* **2020**, *31*, 100958. [[CrossRef](#)]
133. Yin, J.; Yang, L.L.; Yang, X.; Zhu, H.; Wang, D.; Ke, L.; Wang, Z.; Wang, G.; Zeng, X. High-power laser-matter interaction during laser powder bed fusion. *Addit. Manuf.* **2019**, *29*, 100778. [[CrossRef](#)]
134. Zhou, G. Nucleation-induced kinetic hindrance to the oxide formation during the initial oxidation of metals. *Phys. Rev. B Condens. Matter. Mater. Phys.* **2010**, *81*, 1–7. [[CrossRef](#)]
135. Tan, J.H.; Wong, W.L.E.; Dalgarno, K.W. An overview of powder granulometry on feedstock and part performance in the selective laser melting process. *Addit. Manuf.* **2017**, *18*, 228–255. [[CrossRef](#)]
136. Ji, L.; Wang, C.; Wu, W.; Tan, C.; Wang, G.; Duan, X.M. Spheroidization by plasma processing and characterization of stainless steel powder for 3D printing. *Metall. Mater. Trans. A* **2017**, *48*, 4831–4841. [[CrossRef](#)]
137. Simchi, A.; Ahmadi, R.; Reihani, S.M.S.; Mahdavi, A. Kinetics and mechanisms of nanoparticle formation and growth in vapor phase condensation process. *Mater. Des.* **2007**, *28*, 850–856. [[CrossRef](#)]
138. Vermeij, T.; Plancher, E.; Tasan, C.C. Preventing damage and re deposition during focused ion beam milling: The “umbrella” method. *Ultramicroscopy* **2018**, *186*, 35–41. [[CrossRef](#)]
139. Santecchia, E.; Mengucci, P.; Gatto, A.; Bassoli, E.; Denti, L.; Gheorghiu, B.; Barucca, G. Enhancing the Quality of Metal Powder Feedstock for Laser PBF Through Cross-contamination Removal. In Proceedings of the Euro PM2019 Congress, Maastricht, The Netherlands, 13–16 October 2019.

